Available online at www.sciencedirect.com
SCIENCE DIRECT
ELSEVIER
Virology 346 (2006) 74 – 85
VIROLOGY
www.elsevier.com/locate/yviro

SARS coronavirus 7a protein blocks cell cycle progression at G0/G1 phase via the cyclin D3/pRb pathway

Xiaoling Yuan [1], Jie Wu [1], Yajun Shan, Zhenyu Yao, Bo Dong, Bo Chen, Zhenhu Zhao, Shenqi Wang, Jiapei Chen, Yuwen Cong *

Department of Pathophysiology, Beijing Institute of Radiation Medicine, No. 27 Taiping Road, Beijing 100850, China

Received 10 March 2005; returned to author for revision 29 August 2005; accepted 10 October 2005
Available online 21 November 2005

Abstract

The genome of severe acute respiratory syndrome-associated coronavirus (SARS-CoV) contains four structural genes that are homologous to genes found in other coronaviruses, and also contains six subgroup-specific open reading frames (ORFs). Expression of one of these subgroup-specific genes, ORF7a, resulted in apoptosis via a caspase-dependent pathway. Here, we observed that transient expression of ORF7a protein fused with myc or GFP tags at its N or C terminus inhibited cell growth and prevented BrdU incorporation in different cultural cells, suggesting that ORF7a expression may regulate cell cycle progression. Analysis by flow cytometry demonstrated that ORF7a expression was associated with blockage of cell cycle progression at G0/G1 phase in HEK 293 cells after 24 to 60 h post-transfection. Similar results were observed in COS-7 and Vero cells. Mutation analysis of ORF7a revealed that the domain spanning aa 44–82 of 7a protein was essential for its cytoplasmic localization and for induction of the cell cycle arrest. After analyzing the cellular proteins involving in regulation of cell cycle progression, we demonstrated that ORF7a expression was correlated with a significant reduction of cyclin D3 level of mRNA transcription and expression, and phosphorylation of retinoblastoma (Rb) protein at ser795 and ser809/811, not with the expression of cyclin D1, D2, cdk4 and cdk6 in HEK 293 cells. These results suggest that the insufficient expression of cyclin D3 may cause a decreased activity of cyclin D/cdk4/6, resulting in the inhibition of Rb phosphorylation. Accumulation of hypo- or non-phosphorylated pRb thus prevents cell cycle progression at G0/G1 phase.

Keywords: SARS-CoV ORF7a; Growth inhibition; G0/G1 cell cycle arrest; Cyclin D3; Rb phosphorylation; Truncated mutants

Introduction

Severe acute respiratory syndrome (SARS), caused by SARS coronavirus (SARS-CoV), is a life-threatening emerging infectious disease originated from Guangdong Province, China (Poutanen et al., 2003; Tsang et al., 2003). SARS coronavirus (SARS-CoV), a distant member of Group 2 coronaviruses, has recently been identified as the etiological agent of SARS (Drosten et al., 2003; Ksiazek et al., 2003; Marra et al., 2003; Rota et al., 2003). The genome of SARS-CoV is about 29.7 kb with the characteristic gene order [5′-replicase (rep), Spike (S), Envelope (E), Membrane (M), Nucleocapsid (N)-3′]. Besides the four structural proteins, it also contains six open reading frames (ORFs) located between S and E, and M and N genes. The proteins encoded by these ORFs, referred as subgroup-specific ORFs of SARS-CoV show no significant homologies to any previously known proteins (Marra et al., 2003; Rota et al., 2003). Previous studies suggest that coronavirus accessory proteins, varying in size and position in the genome of coronaviruses, may be dispensable for virus replication, at least in the cell culture system, and important for virus–host interaction. For example, mutation or deletion of one of these proteins, such as ORF7b of feline coronavirus and ORF3 of swine enteric and respiratory coronavirus is related to their reduced virulence and pathogenesis (Herrewegh et al., 1995; Paul et al., 1997).

Expression of SARS-CoV ORF7a (CDS: 27273–27639), also referred as ORF8, X4 and U122 was confirmed in the

Abbreviations: SARS, severe acute respiratory syndrome; SARS-CoV, SARS-associated coronavirus; HEK, human embryonic kidney; DMEM, Dulbecco's modified Eagle medium; pRb, phosphorylated-retinoblastoma; cdk, cyclin-dependent kinase; ORF, open reading frame; BrdUrd, 5-Bromodeoxyuridine; MTT, 3-(4,5-dimethylthiazol-2-yl)-2,5-dipheyl tetrazolium bromide.

* Corresponding author. Fax: +86 10 68214653.
E-mail address: congyw@nic.bmi.ac.cn (Y. Cong).
[1] These authors contributed equally.

0042-6822/$ - see front matter © 2005 Elsevier Inc. All rights reserved.
doi:10.1016/j.virol.2005.10.015

SARS-CoV infected cells with anti-7a antisera (Fielding et al., 2004; Nelson et al., 2005; Rota et al., 2003; Yount et al., 2003). It was reported that 7a protein was located at ER and ER-Golgi intermembrane compartment and interacted with SARS-CoV ORF3a protein in the SARS-CoV infected Vero E6 cells (Fielding et al., 2004; Nelson et al., 2005; Tan et al., 2004b). Recent data showed that overexpression of 7a protein could induce apoptosis via a caspase-dependent pathway in the transfected cell lines derived from different organs (Tan et al., 2004a). In this article, we first presented the evidence that overexpression of 7a could inhibit cell growth and block cell cycle procession at G0/G1 phase via cyclin D3/Rb pathway, and the domain responsible for these functions was identified through mutation analysis. These results suggest that 7a may play important roles in life cycle of SARS-CoV and the pathogenesis induced by SARS-CoV.

Results and discussion

Growth inhibition of SARS-CoV ORF7a of transfected cells

SARS-CoV ORF7a (ZJ01, AY297028) was cloned into pCMV-myc, pEGFP-N1 and pEGFP-C1 vectors separately and expressed in HEK 293 cells. Western blotting assay with anti-myc antibody demonstrated the expression of myc-7a protein in the transfected cells, which migrated at the expected molecular mass of approximately 19.5 kDa. In GFP-7a expressed cells, the expected band at 48.5 kDa was detected with anti-GFP antibody. However, two bands of ~48.5 kDa and 46 kDa were observed in 7a-GFP transfected cells (Fig. 1A). Published data showed that about 50% of the precursor form of 7a (~17.5 kDa) was cleaved from the signal peptide at the N terminus, yielding a product of ~15 kDa protein in SARS-CoV infected Vero E6 cells (Fielding et al., 2004). The reason for only emergence of unprocessed forms of myc-7a and GFP-7a may be that the tag at N terminus of 7a affects the cleavage of the signal peptide.

We have observed that HEK 293 cells transfected with 7a/pCMV-myc grow slower than pCMV-myc transfected cells. We thus speculated that expression of 7a protein may inhibit cell proliferation. The numbers of both pCMV-myc and 7a/pCMV-myc transfected HEK 293 cells, as quantitated with trypan blue dye exclusion assay, increased significantly from 0 to 24 h post-transfection. But from 24 to 48 h post-transfection, the myc-7a expressed cells grew much slower than the cells expressing myc only, but no 7a protein ($P < 0.05$) (Fig. 1B). Similar growth inhibition of 7a/pEGFP-N1 transfected cells was observed when compared with pEGFP-N1 transfected cells ($P < 0.05$). These results indicate that expression of 7a is associated with inhibition of cell growth. The above experiments were repeated with MTT assay, a more sensitive colorimetric test to monitor the cell proliferation. As shown in Fig. 1C, the growth inhibition of 7a/pCMV-myc transfected HEK 293 cells was significantly dependent on the dose of plasmid used for transfection, whereas the growth of 7a/pCMV-myc transfected HEK 293 cells was marginally inhibited at the highest dose of plasmid (1.25 μg/ml). Flow cytometric analysis revealed that the transfection efficiencies of 7a/pCMV-myc were significantly raised from 10% to 45% with the increase of plasmid doses from 0.25 to 1.25 μg/ml. Similar results were obtained in 7a/pEGFP-N1 and pEGFP-N1 transfected HEK 293 cells (data not shown). These data further suggest that the cell growth inhibition level is correlated with the amounts of 7a expressed in the transfected cells. To address the mechanism of 7a on cell growth inhibition, cell DNA synthesis was further measured by 5-Bromodeoxyuridine (BrdUrd) incorporation. As shown in Fig. 1D, about 75% of 7a-GFP negative cells had BrdUrd incorporation, while most 7a-GFP positive cells partly or completely lacked BrdUrd incorporation in 7a/pEGFP-N1 transfected COS-7 and Vero cells. As a control, both pEGFP-N1 positive and negative cells had similar rates of BrdUrd incorporation. These data indicate that 7a expression inhibits cells growth and prevented cell cycle entry into S phase.

Expression of SARS-CoV ORF7a block cell cycle arrest in G0/G1

Cell cycle dysregulation is a common response of host cells to many virus infections. Cell cycle arrest can be efficiently induced by some viral proteins such as Vpr of human immunodeficiency virus (HIV), ORF-a of feline immunodeficiency virus and p28 of murine hepatitis coronavirus (MHV) (Chen et al., 2004; Gemeniano et al., 2004; He et al., 1995). Flow cytometry is a rapid, quantitative, multiparameter analysis of cells based on the measurement of visible and fluorescent light emission. Using myc-tag as an indicator of the positively transfected cells (Deng et al., 2004), cell cycle profile of two intercultural populations was analyzed by flow cytometry in 7a/pCMV-myc transfected HEK 293 cells. The transfection efficiency of 7a/pCMV-myc in HEK293 cells was revealed to be 36.6% by flow cytometry. As shown in Fig. 2A, about 87% of 7a positive cells were in G0/G1 phase and only ~35% of negative cells were in G0/G1 phase at 24 h post-transfection ($P < 0.01$). As a control, wild-type and pCMV-myc transfected HEK 293 cells had similar cell cycle profiles with about 50% of cells in G0/G1 phase. To reveal the functional integrity of 7a protein, the above experiments were repeated with 7a fused with GFP tag at its C or N terminus. The transfection efficiencies of pEGFP-N1, 7a/pEGFP-N1 and 7a/pEGFP-C1 in HEK293 cells were about 20%, 30.0% and 29.0%, respectively. As expected, the pEGFP-N1 transfected cells showed similar cell cycle profiles between GFP positive and negative cells, but the percentage of G0/G1 phase in 7a/pEGFP-N1 positive cells (83%) was greater than that in the negative ones (29%), suggesting that 7a expression could block cell cycle progression at G0/G1 phase ($P < 0.01$). While in 7a/pEGFP-C1 transfected cells, the blockage of G0/G1 phase was also observed, but was less significant than that in 7a/pEGFP-N1 transfected cells, suggesting that GFP fusion at the N terminus of 7a may partly impact its function. To observe whether the G0/G1 phase arrest induced by 7a expression was cell line-specific or not, pCMV-myc and 7a/pCMV-myc were separately transfected into COS-7 and Vero cells. COS-7 was

another higher transfection efficiency cell line that derived from African green monkey kidney. Vero cells, derived from African green monkey kidney fibroblast-like, were susceptible to SARS-CoV infection. Like HEK 293 cells, transfection with pCMV-myc had little effects on cell cycle profiles of COS-7 and Vero cells (data not shown). In both cells, G0/G1 phase arrests induced by 7a expression were observed which was as obvious as that in HEK 293 cells, indicating that some common proteins in different cell lines were involved in the G0/G1 phase arrest induced by 7a expression (Fig. 2B). Similar results were observed in 7a/pEGFP-N1 transfected COS-7 and Vero cells (data not shown).

The G0/G1 phase arrest is a crucial DNA damage checkpoint, which acts as an important safeguard for genomic stability. Cells in G0/G1 phase arrest might go into apoptosis, or recover from the G0/G1 phase and entering into S phase (Chen et al., 2004; Deng et al., 2004). To observe the denouement of the G0/G1 phase arrest induced by 7a protein, cell cycle analysis was performed in 7a/pCMV-myc transfected HEK 293 cells from 24 to 60 h after transfection. It was shown that increases in G0/G1 phase and decreases in S phase in myc-7a expressed cells were obvious throughout all times, and more significant at 24 h post-transfection ($P < 0.01$). With the increases in S phase at the late time points, the percentage of G0/G1 phase became decreased in myc-7a expressed cells. Sub-G1 phases, representing one type of cell apoptosis, were observed at late time points, but not over 10% of analyzed cells. Interestingly, there was no significant difference in sub-G1 phase between myc-7a positive and negative cells (Fig. 2C). Redistribution of phosphatidylserine is an early and common phenomenon in the process of cell apoptosis, which can be stained by Annexin V. HEK 293 cells were harvested at 24 h, 36 h and 48 h after transfection with pCMV-myc and 7a/pCMV-myc, and apoptosis was measured by using Annexin V staining. The transfection efficiency of 7a/pCMV-myc in HEK293 cells was revealed to be about 40% by flow cytometry. Fluorescence-activated cell sorting analysis indicated that the rates of apoptosis at 24 h, 36 h and 48 h post-transfection were 9.4%, 8.5% and 10.0% in 7a/pCMV-myc transfected cells and 3.8%, 3.4% and 3.0% in pCMV-myc transfected cells (Fig. 2D). It was reported that overexpression of ORF7a could induce apoptosis via a caspase-dependent pathway (Tan et al., 2004a). However, the data from our results support the opinion that 7a protein may be much more a cell cycle arrest inductor than an apoptosis inductor.

Cellular localization and G0/G1 cell cycle arrest induction of SARS-CoV ORF7a truncated mutants

Sequence analysis using PSORT II software predicted that ORF7a, encoding a type I transmembrane protein, 122 amino acids (aa) in length, consists of a 15 residue signal peptide at its N terminus, an 81 residue luminal domain, a 17 residue transmembrane segment (from 101 to 117 aa) and ER membrane retention signals (KRKTE) at its C-terminus (Fielding et al., 2004; Hofmann and Hadge, 1987). To define the functional domain of 7a protein for inducing cell cycle arrest, a series of truncated mutants from C-terminus of 7a were constructed based on the bioinformation obtained from the bioinformation analysis to avoid major disruption of protein folding (Fig. 3A). The genes for encoding the 7a mutants, D118–122, D102–122, D83–122 and D44–122 with deletion of the KRKTE ER retrieval signal, the transmembrane region, the proximal membrane region and the middle domain of 7a, respectively, were cloned into pCMV-myc vector separately. These truncated 7a proteins expressed in the transfected cells showed the expected molecular mass in Western blotting assays (data not shown). The subcellular localization of these deleting constructs was performed in HEK 293 cells. As shown in Fig. 3B, wild-type 7a was observed to distribute in the cytoplasm and plasma membrane in a punctulate pattern with condensing into discrete loci and spot fluorescence. The mutants D118–122, D102–122 and D83–122 had similar fluorescent distribution as wild-type 7a protein; however, D44–122 displayed a more smear fluorescence in cytoplasm and nucleus, indicating that the domain spanning aa 44–82 was needed for 7a cytoplasm localization.

The cell cycle analysis was performed as before in HEK 293 cells. At 24 h post-transfection with 7a-mutants/pCMV-myc and pCMV-myc plasmids, cells were collected and analyzed by flow cytometry. The transfection efficiencies in the ORF7a, D118–122, D102–122, D83–122 and D44–122 transfected cells were 45.7%, 35.6%, 40.1%, 37.6% and 82.0%, respectively. As shown in Fig. 3C, when compared with pCMV-myc transfected cells, mutant D118–122, D102–122, D83–122 and

Fig. 1. 7a expression inhibited cell growth in different cells. (A) Western blotting analysis. HEK 293 cells were transiently transfected with pCMV-myc, 7a/pCMV-myc, pEGFP-N1, 7a/pEGFP-N1, pEGFP-C1 and 7a/pEGFP-C1 plasmid separately. Cell lysates were prepared at 48 h after transfection and detected with anti-GFP or anti-myc antibody. Sizes (kDa) of molecular mass were indicated on the right. (B) Growth inhibition of 7a protein in transfected cells. HEK 293 cells were transfected with equivalent amounts of pCMV-myc, 7a/pCMV-myc, pEGFP-N1 or 7a/pEGFP-N1 separately. At 12, 24, 36, 48 and 60 h after transfection, samples were collected. Viable cells, which were resistant to staining of trypan blue, were counted using hemacytometer chamber. Cell counts at each time point were the mean values of three independent experiments with standard deviation. (C) Effects of different amounts of pCMV-myc or 7a/pCMV-myc vectors on the growth of the transfected cells. HEK 293 cells were transfected with different concentration of pCMV-myc or 7a/pCMV-myc in 96-well culture plates. After 48 h, each well was supplemented with methylthiazol tetrazolium (MTT) solution and the optical density (O.D.) was measured at 540 nm. The experiments were independently repeated three times and one experiment was presented with three duplicates at each concentrations. (D) Overexpression of 7a inhibited DNA replication of COS-7 and Vero cells. At 24 h after transfection with pEGFP-N1 or 7a/pEGFP-N1, COS-7 and Vero cells on glass slips were incubated with 10 μmol/l BrdUrd and stained with anti-BrdUrd and anti-GFP antibodies. Images were viewed with confocal fluorescent microscope. The left panel displayed the GFP positive cells, the middle panel showed the BrdUrd incorporation cells and the right panel displayed the overlay of BrdUrd and 7a-GFP or GFP staining images.

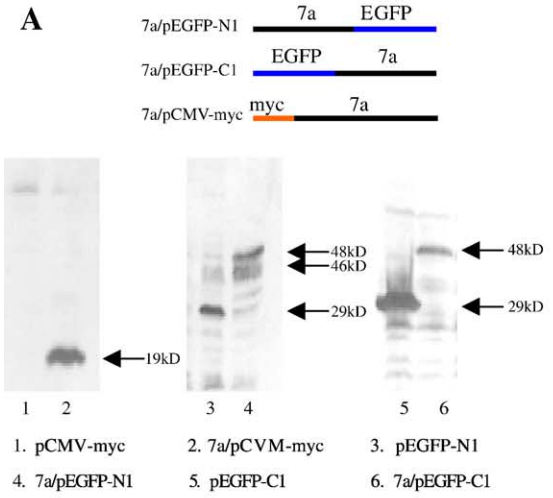
A
7a/pEGFP-N1
7a
EGFP
7a/pEGFP-C1
EGFP
7a
7a/pCMV-myc
myc
7a
19kD
48kD
46kD
29kD
48kD
29kD
1 2 3 4 5 6
1. pCMV-myc
2. 7a/pCVM-myc
3. pEGFP-N1
4. 7a/pEGFP-N1
5. pEGFP-C1
6. 7a/pEGFP-C1

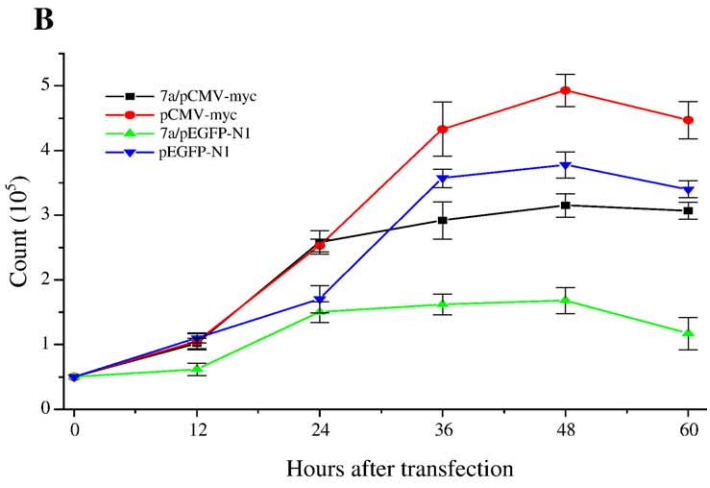
B
7a/pCMV-myc
pCMV-myc
7a/pEGFP-N1
pEGFP-N1
Count (10^5)
0
1
2
3
4
5
0
12
24
36
48
60
Hours after transfection

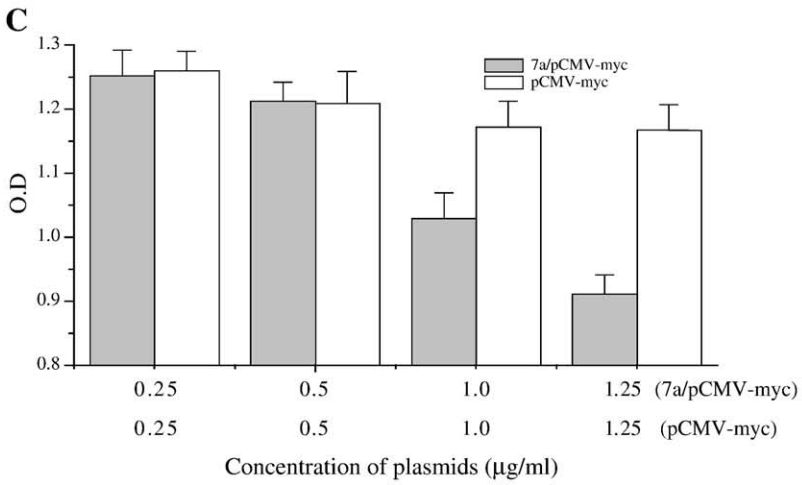
C
7a/pCMV-myc
pCMV-myc
O.D
0.8
0.9
1.0
1.1
1.2
1.3
0.25 0.5 1.0 1.25 (7a/pCMV-myc)
0.25 0.5 1.0 1.25 (pCMV-myc)
Concentration of plasmids (μg/ml)

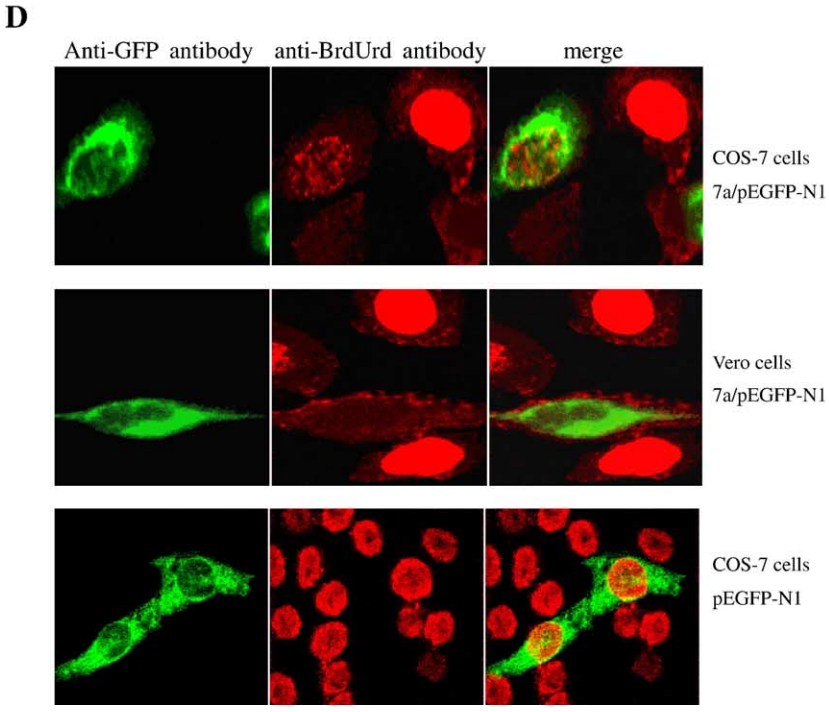
D
Anti-GFP antibody
anti-BrdUrd antibody
merge
COS-7 cells
7a/pEGFP-N1
Vero cells
7a/pEGFP-N1
COS-7 cells
pEGFP-N1

7a had a similar ability in inducing cell G0/G1 arrest ($P < 0.05$), while D44–122 had little effect on cell cycle progression (Fig. 3C), suggesting that the middle domain from 44 to 82 aa was required for blocking cell cycle progression at G0/G1 phase. A point to note was that cell G0/G1 phase arrest in D118–122 expressed cells was less obvious than that in D102–122 and

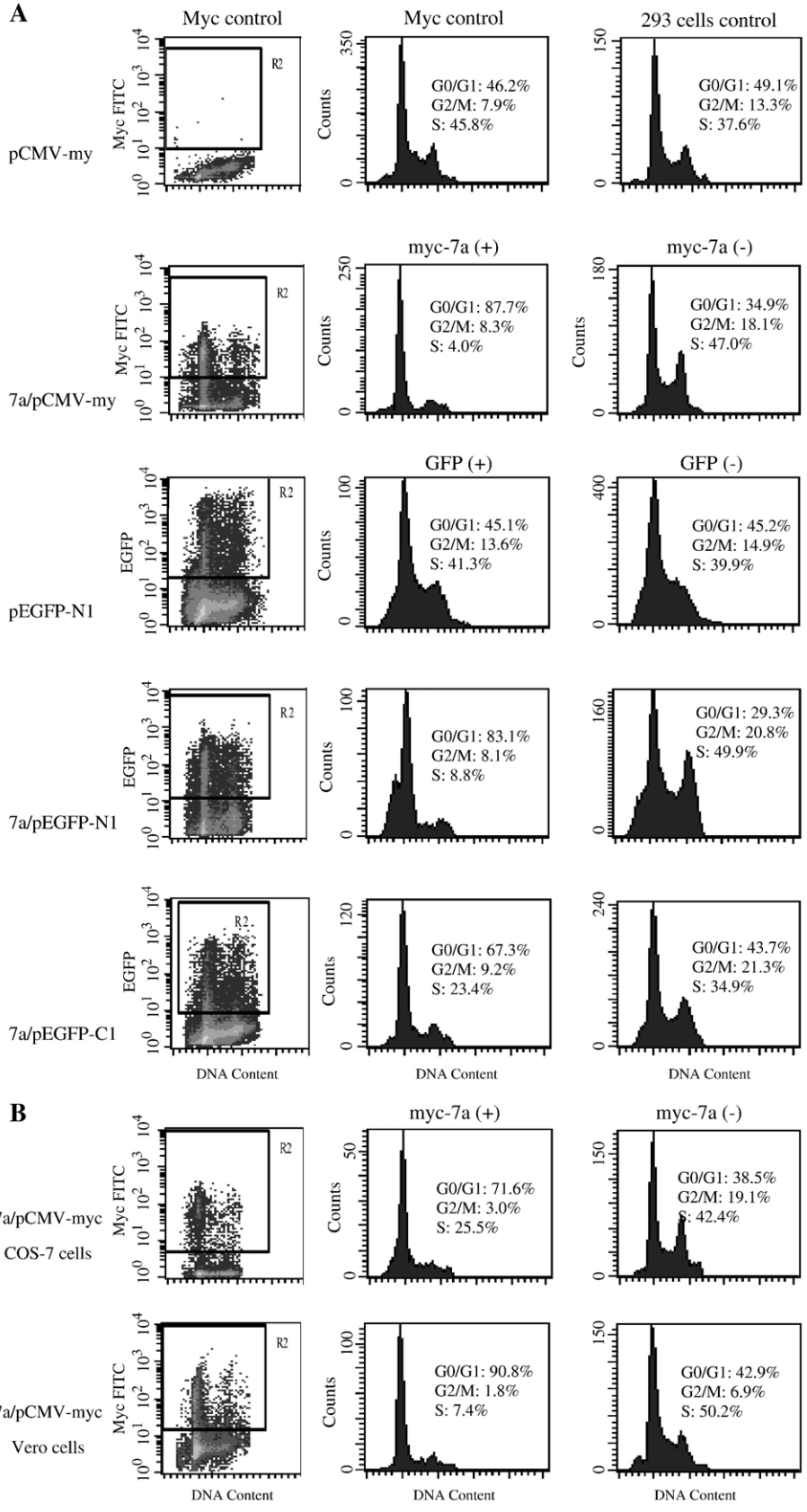

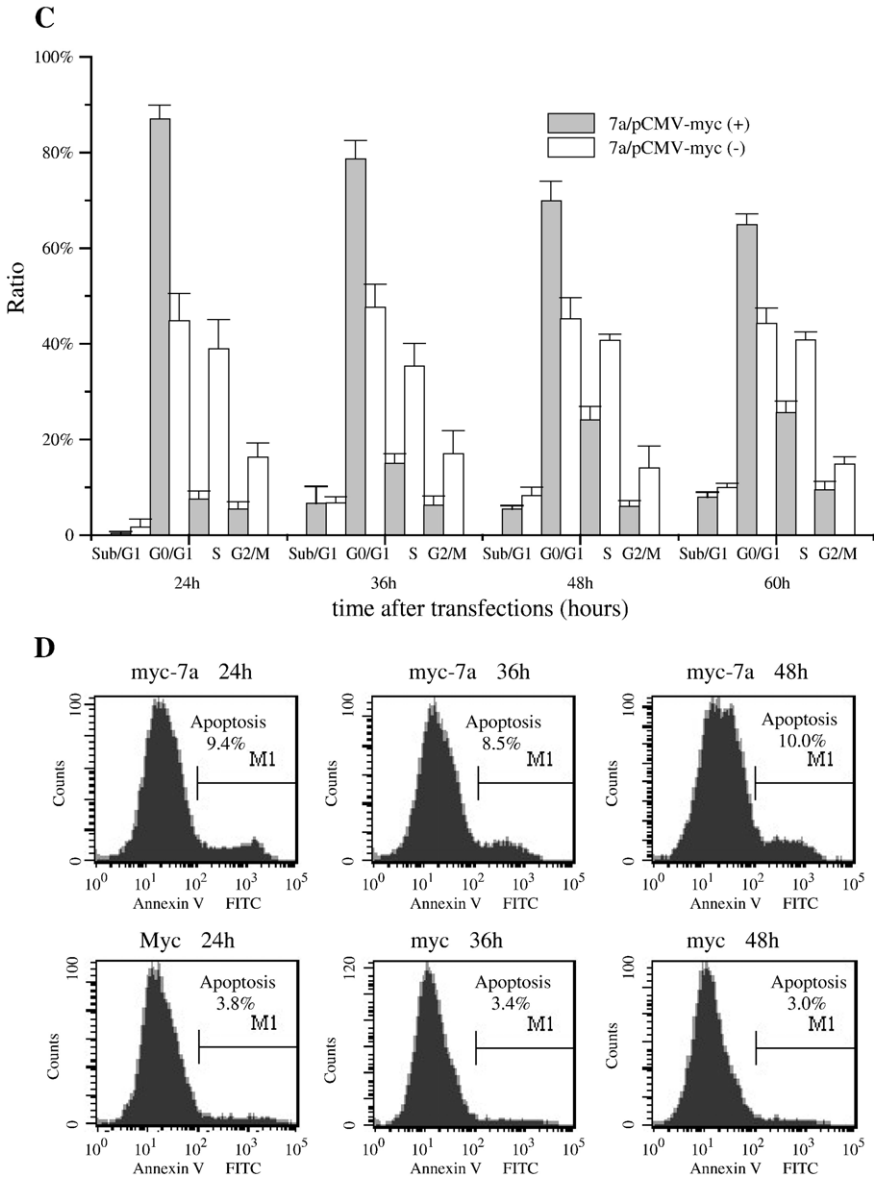

Fig. 2. 7a expression blocked cell cycle progression at G0/G1 phase. (A) Expression of 7a fused with different tags induced G0/G1 cell cycle arrest. pCMV-myc, 7a/pCMV-myc, pEGFP-N1, 7a/pEGFP-N1 and 7a/pEGFP-C1 plasmids were transfected into HEK 293 cells separately. At 24h post-transfection, samples were collected and stained with propidium iodide (PI). The DNA contents of cells were measured by flow cytometry. Myc-7a (+) viewed with anti-myc antibody and EGFP (+) represented the positive cells (myc-7a or EGFP fusion protein expressed cells) in the middle column, and myc-7a (−) and EGFP (−) represented negative cells in the right column in the transfected cells. The experiments were independently repeated three times. (B) Cell cycle arrest induced by 7a expression in COS-7 and Vero cells. 7a/pCMV-myc plasmid was transfected into COS-7 and Vero cells. At 24 h after transfection, the DNA contents of cells were analyzed by flow cytometry as before. Three independent sets of experiments were repeated. (C) Cell cycle arrest induced by 7a expression at different times post-transfection. HEK 293 cells were transfected with 7a/pCMV-myc and pCMV-myc. At 24, 36, 48 and 60 h after transfection, samples were collected and analyzed by flow cytometry as before. Myc-7a positive and negative cells were showed with gray and white bars. Histogram was shown the percentages of cells at various phase of cell cycle with means ± SE for three independent sets of experiments. (D) Profile of Annexin V staining in 7a/pCMV-myc and pCMV-myc transfected cells. HEK 293 cells were transfected with 7a/pCMV-myc and pCMV-myc. At 24, 36 and 48 h post-transfection, samples were collected and analyzed by flow cytometry for the ability to bind Annexin V according to the manufacture's guidelines (Clontech).

D83–122 expressed cells. This was likely due to the low transfection efficiency of D118–122/pCMV-myc plasmid. Using Annexin V staining, the rates of apoptosis in the ORF7a, D118–122, D102–122, D83–122, D44–122 and pCMV-myc transfected HEK 293 cells were 8.5%, 10.3%, 7.0%, 8.3%, 3.6% and 3.4%, respectively (Fig. 3D). These results suggested that the domains for inducing cell cycle arrest and apoptosis seem located to the same region of 7a protein.

G0/G1 cell cycle arrest induction of SARS-CoV 7a via the cyclin D3/pRb pathway

One key regulator of cell cycle progression from the G0/G1 phase to the S phase is Rb, which binds to and represses the transcription factor E2F. The hyperphosphorylation of Rb by some cyclin/cdk complexes allows the release and activation of E2F, permitting the transcription of S phase genes. It was

reported that phosphorylation of Rb on Ser-795 is important for its binding to E2F and phosphorylation of Rb on Ser-807/811 is needed to bind the ubiquitously expressed c-Abl tyrosine kinase (Dimberg et al., 2003). To understand the mechanism of 7a-induced G0/G1 cell cycle arrest, we first examined the phosphorylation status of Rb in transfected cells by Western

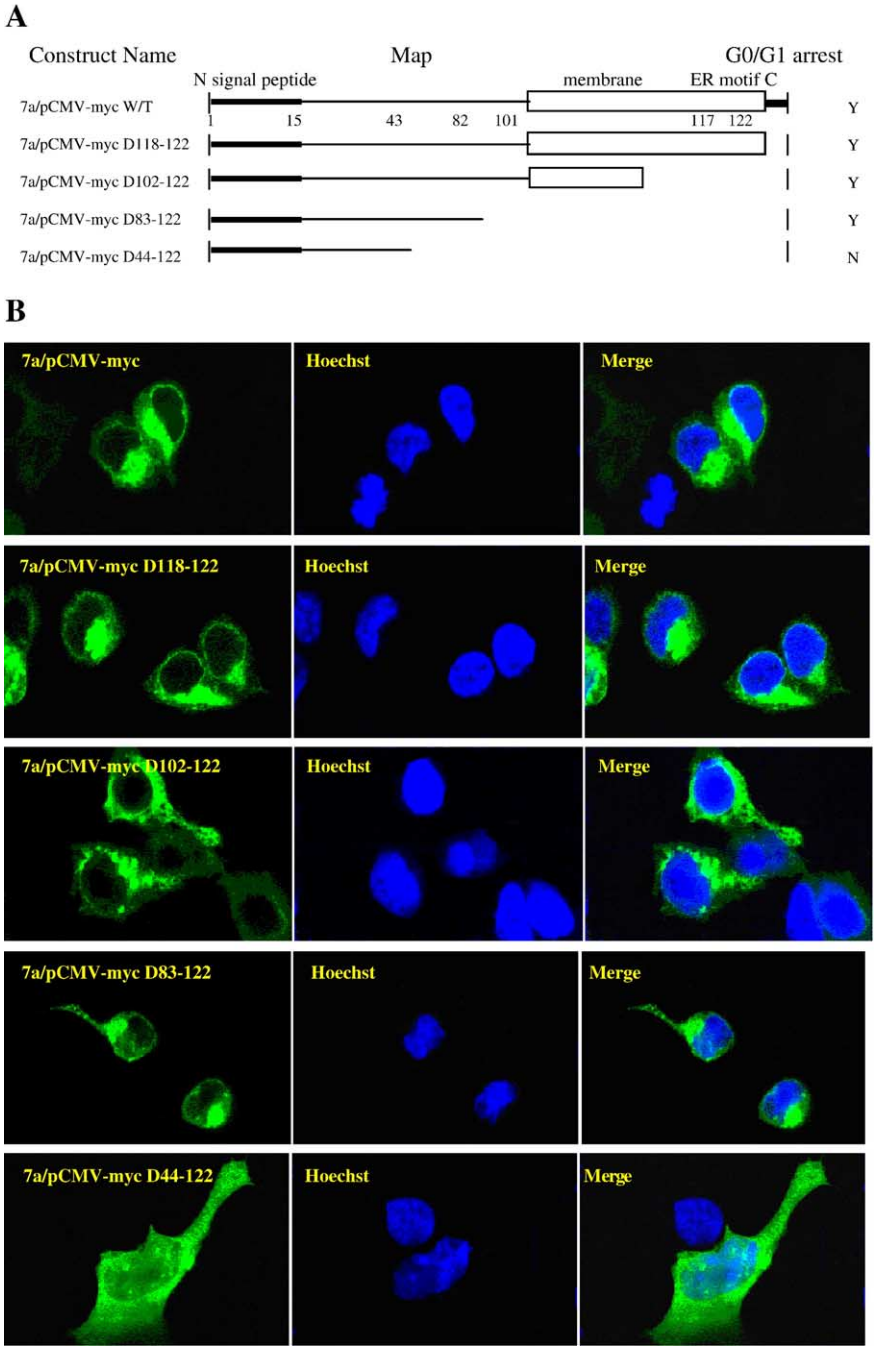

Fig. 3. Cellular localization and cell cycle arrest induction of 7a truncated mutants. (A) Schematic representation of ORF7a truncated mutants. The different mutants of ORF7a were constructed based on bioinformatic analysis of 7a. The box represented the transmembrane domain referred to as membrane, and the black bars at N or C terminus were represented the signal peptide and KRKTE ER retrieval signal motif, respectively. The amino acid positions for ORF7a mutants were given below, the statuses of G0/G1 phase arrest were shown on the right. (B) Cellular localization of 7a truncated mutants. Serial mutants of ORF7a (D118–122, D102–122, D83–122 and D44–122) cloned to pCMV-myc vector were transfected into HEK 293 cells. At 24 h after transfection, the cells on glass slips were fixed and viewed with anti-myc antibody. The nuclear was stained with Hoechst. Cellular localization was observed by scanning fluorescence confocal microscopy. Green (on the left) represented expression of mutant 7a; blue (in the middle) represented Hoechst stained cell nuclei; and images (on the right) represented overlapping green and blue fluorescence. (C) Expression of 7a mutants blocked cell cycle progression at G0/G1 phase. HEK 293 cells were transfected with described constructs of ORF7a separately. At 24 h post-transfection, samples were collected and stained with PI. DNA contents of cells were measured by flow cytometry. Three independent sets of experiments were repeated. (D) Profile of Annexin V staining in ORF7a mutants transfected cells. HEK 293 cells were transfected with ORF7a mutants. At 24 h post-transfection, samples were collected and analyzed by flow cytometry for the ability to bind Annexin V as before.

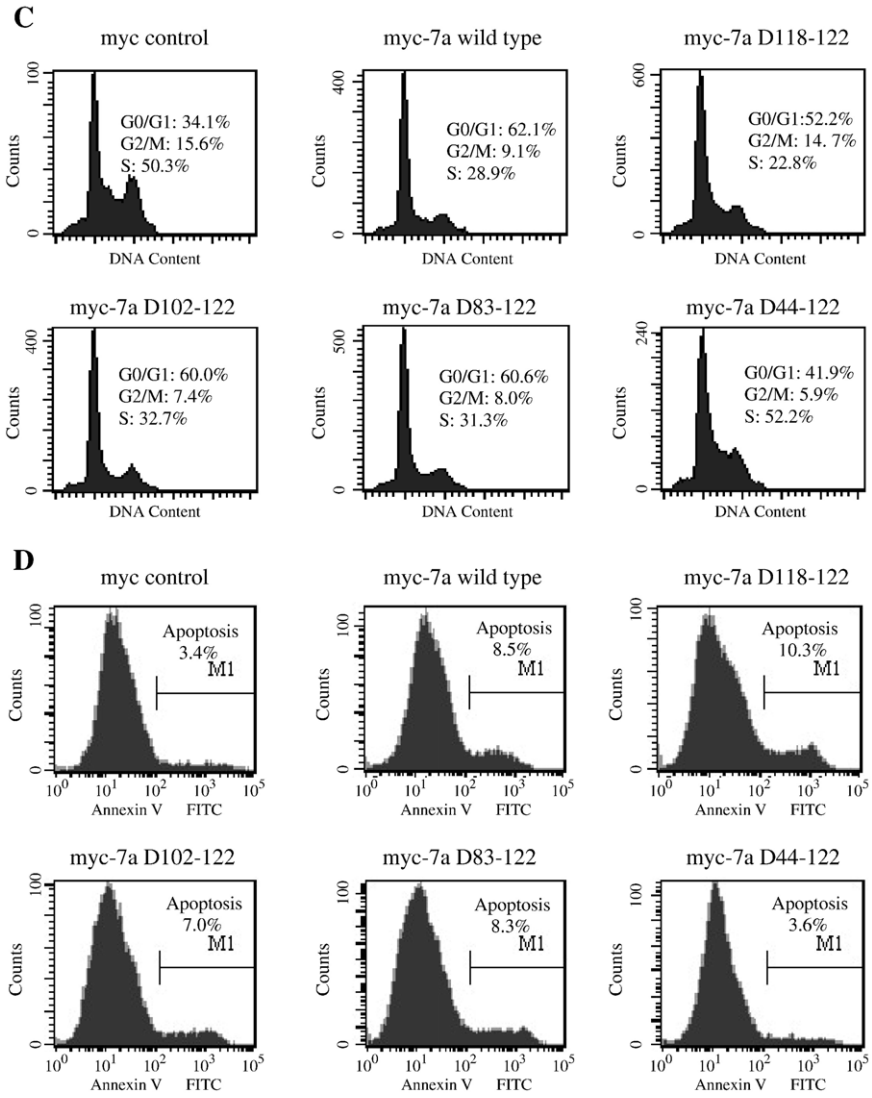

Fig. 3 (*continued*).

blotting analysis. The total HEK 293 cells transfected with pCMV-myc, 7a/pCMV-myc, pEGFP-N1 and 7a/pEGFP-N1 plasmids were collected at 24 h post-transfection and analyzed with phosphor-specific anti-Rb antibodies on Ser-795 or Ser-807/811. As shown in Fig. 4A, GFP, 7a-GFP and myc-7a were expressed at the expected molecular mass and Rb phosphorylation on Ser-795 and Ser-807/811 was down-regulated in 7a-GFP and myc-7a expressed cells. It was indicated that the expression of 7a, rather than myc or GFP, inhibits Rb phosphorylation and blocks cell cycle progression at G0/G1 phase. The phosphorylation status of Rb was further studied in 7a/pCMV-myc transfected cells (Fig. 4B). Expression of myc-7a was observed at all the time points with the highest level at 24 h post-transfection, whereas the phosphorylation of Rb on ser795 and ser807/811 decreased gradually after transfection. Same density of the actin bands were revealed, suggesting that the varied levels of the expression of 7a and phosphorylation of Rb are not due to the different amounts of total cell lysates loaded. More obvious G0/G1 phase arrest (Fig. 2C) at 24 h post-transfection was coincided with the higher level of 7a expression, but not with the phosphorylation status of Rb, suggesting that multiple pathways may be involved in the regulation of cell cycle.

G1 cyclin/cdk complexes regulate cell cycle progression through the phosphorylation of Rb. pRb is hypo-phosphorylated by cyclin D/cdk4/6 complexes in early G1 phase and hyper-phosphorylated by the cyclin E/cdk2 complex in late G1 phase, followed by a continuous hyper-phosphorylation in the S, G2 and M phases of cycling cells. Chen and Makino (2004) first reported that infection of coronavirus MHV inhibited Rb phosphorylation and induced cell cycle arrest through the reduction of cdk4, cdk6 and G1 cyclins such as D1, D2, D3 and E. Accordingly, the inhibition of Rb phosphorylation in 7a expressed cells suggests that the expression of G1 cyclin/cdk complexes was suppressed. To verify the possibility, we have analyzed the expression levels of cyclin D1, D2, D3 and cdk4, cdk6 in 7a/pCMV-myc and 7a/pEGFP-N1 transfected cells by Western blots. No significant changes were observed in the levels of cdk4 and cdk6 between pCMV-myc and 7a/pCMV-myc, and between

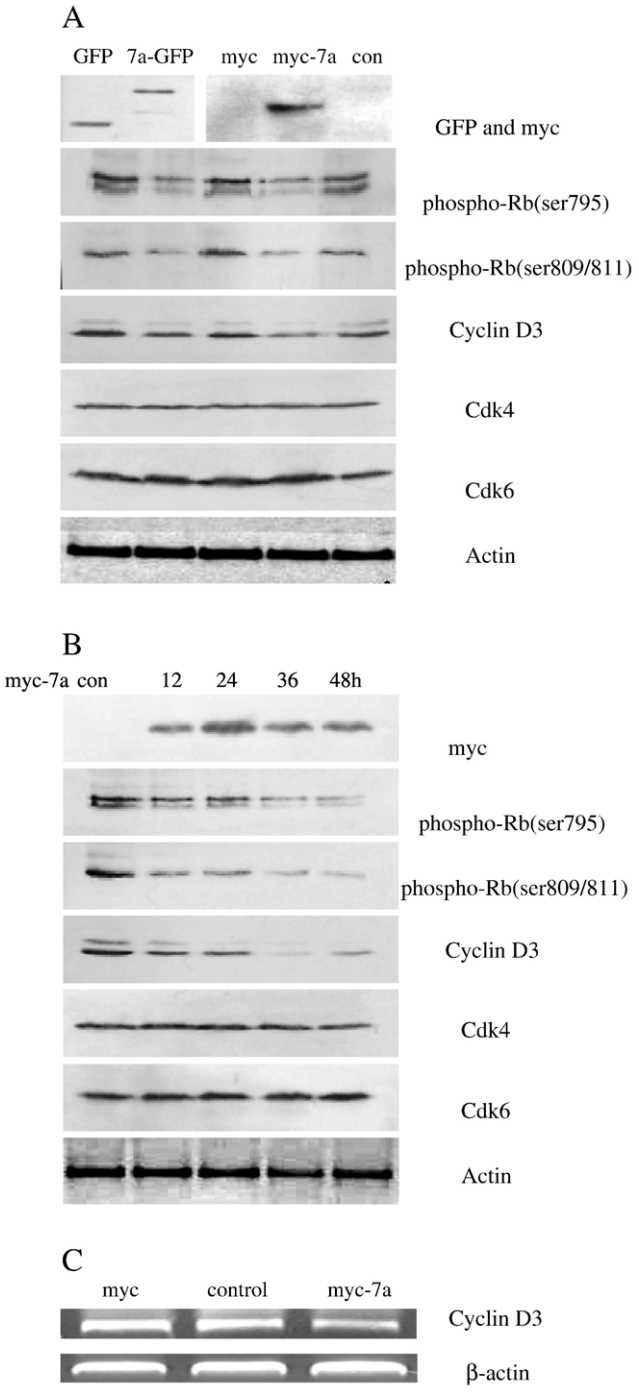

Fig. 4. 7a expression affects the phosphorylation status of Rb and levels of G1 cdks and cyclins. (A) HEK 293 cells were transfected with equivalent amounts of pCMV-myc, 7a/pCMV-myc, pEGFP-N1 or 7a/pEGFP-N1 plasmid separately. At 24 h after transfection, cell lysates were prepared and probed with primary antibodies as given, and visualized by enhanced chemiluminescence (ECL) reagents. (B) HEK 293 cells were transfected with equivalent amounts of pCMV-myc and 7a/pCMV-myc plasmids separately. At 12, 24, 36 and 48 h after transfection, cell lysates were prepared and viewed as before. (C) After transfection with equivalent amounts of pCMV-myc and 3a/pCMV-myc separately, the total RNA prepared from the HEK 293 cells was used for RT-PCR with primers of cyclin D3 and β-actin. PCR products were separated on 1.2% agarose gel.

pEGFP-N1 and 7a/pEGFP-N1 transfected cells (Fig. 4A). And the expression of cdk4 and cdk6 was not obviously different from 12 to 48 h after transfection with 7a/pCMV-myc (Fig. 4B). In contrast, cyclin D3 was markedly decreased in myc-7a or 7a-GFP expressed cells when compared with control ones. Furthermore, the level of cyclin D3 was significantly decreased from 12 to 48 h after transfection with 7a/pCMV-myc, which was consistent with the changes of Rb phosphorylation. The expression of cyclin D1 and D2 was not observed in HEK 293 transfected with 7a/pCMV-myc, pCMV-myc, 7a/pEGFP-N1 and pEGFP-N1, respectively (data not shown). Using the same antibodies, the expression of cyclin D1 and D2 was observed in NIH/3T3 cells and A549 cells, respectively. So, the reason for not detecting the changes of cyclin D1 and D2 in our tests may be that the amounts of these proteins in HEK 293 cells were too small to detect. In addition, transcription of cyclin D3 mRNA was analyzed by RT-PCR assay. As compared with the control cells, the transcriptional level of cyclin D3 was decreased obviously in 3a/pCMV-myc transfected cells (Fig. 4C). It was indicated that the decrease in the amounts of cyclin D3 induced by ORF7a expression may come from the down-regulation of its mRNA transcription. The activities of G1 cyclin/cdk complexes are regulated by cdk-inhibitors (CKIs), which can be grouped into INK4 family and Cip/Kip family (Sherr and Roberts, 1999). To gain further insight into the nature of the cell cycle arrest induced by 7a protein, the expression levels of $p21^{Cip1}$ and $p27^{Kip1}$, two main members of Cip/Kip family, were examined in the 7a/pCMV-myc and 7a/pEGFP-N1 transfected HEK 293 cells by Western blotting. 7a expression had no effect on the amounts of p21 and p27 proteins (data not shown). As a control, the activation of cyclin A/cdc2 complex, which is an important regulatory complex in G2/M phase, was further examined. It was shown that there were no changes in the status of phosphorylated cdc2 as well as expression of cyclin A in 7a transfected cells (data not shown). These results suggest that significant reduction of cyclin D3 induced by 7a expression prevents activity of the cyclin D/cdk4/6 complex in HEK 293 cells, which in turn may cause the inhibition of the phosphorylation of Rb, resulting in blockage of the cell cycle progression in the G0/G1 phase.

Three cyclins (cyclin D1, D2 and D3) have been identified in mammalian cells. Cyclin D3 is expressed in nearly all of proliferating cells, and it is the most broad expression pattern of the three D-type cyclins. Sicinska et al. (2003) reported that cyclin D3−/− mice suffered from an isolated defect in thymocyte development characterized by a marked deficit in $CD_4^+CD_8^+$ double positive T cells. The significant decreases in peripheral CD_4^+ and CD_8^+ T lymphocyte subsets observed in SARS patients are related to the onset of SARS (Huang et al., 2005). The mechanism for this lymphocytopenia induced by SARS-CoV infection is largely unknown. Angiotensin-converting enzyme 2 (ACE2) and CD209L, two potential SARS-CoV receptors, were reported to be expressed in lymph nodes, thymus and Peyer's patches, and proposed to mediate transfer of SARS-CoV to T cells (Jeffers et al., 2004; Li et al.,

2003). Therefore, it would be interesting to test whether 7a expression induces growth inhibition or apoptosis of T lymphocytes via the reduction of cyclin D3.

The role of cell cycle arrest induced by 7a was not determined in viral life cycle of SARS-CoV, but proposed from recent relative studies. Infection by coronavirus MHV resulted in inhibition of host cellular DNA synthesis and accumulation of cells in G0/G1 phase in activating DBT and 17Cl-1 cells through inducing cyclin D2 and cyclin E degradation (Chen and Makino, 2004). The expression of non-structural protein p28 of MHV may be responsible for induction of G0/G1 phase arrest and cell cycle arrest (Chen et al., 2004). Increasing data suggest that cell cycle arrest in the G0/G1 phase may favor coronavirus replication and exacerbate virus-induced pathogenicity, especially in some aspects, such as increasing amounts of ribonucleotide pools for efficient coronavirus RNA synthesis, preventing the induction and execution of early cell death in infected cells, assisting in efficient coronavirus assembly, benefiting cap-dependent translation of coronavirus proteins and decreasing the killed efficiency of coronavirus infected cells by cytotoxic T cells (Bonneau and Sonenberg, 1987; Chen and Makino, 2002, 2004; Nishioka and Welsh, 1994). The present study has shown that expression of 7a could significantly inhibit cell growth and induce cell G0/G1 phase arrest through cyclin D3/pRb pathway, suggesting that 7a may play an important role in SARS-CoV induced pathogenesis.

Materials and methods

Cell culture and transfection

HEK 293 (human embryonic kidney) cells, Vero (African green monkey kidney) cells and COS-7 (African green monkey kidney) cells were grown in Dulbecco's modified Eagel medium (DMEM) (Gibco BRL) supplemented with 10% FBS at 37 °C in a incubator supplied with 5% CO_2. When cell density in a culture plate reached 70% confluence, the cells were transfected with different plasmid DNA using Lipofectamine 2000 (Invitrogen) following the protocol provided by the manufacturer. In brief, total amount of DNA transfected into the cells in each well was adjusted to 1.5 μg/ml by using empty pCMV-myc vector. Cells were incubated with transfection mixtures for 5 h and then replaced with the fresh medium.

Construction of expression vectors of SARS-CoV 7a and its mutants

The orf7a gene was PCR-amplified from the SARS-CoV (ZJ01, AY297028) genome using *Taq* DNA polymerase (NEB). PCR was performed with a forward primer (containing a *Xho*I site) complementary to the 5′ end of the ORF7a and a reverse primer (containing a *Eco*RI site) complementary to the 3′ end of the ORF7a but without stop codon to allow for read-through (Table 1). This product was cut with *Xho*I and *Eco*RI and cloned into the multiple cloning site (MCS) of the pEGFP-N1 vector (Clontech), producing a 7a/pEGFP-N1 plasmid. The plasmid was confirmed by sequencing. The 7a/pEGFP-C1, 7a/pCMV-myc and serial 7a mutants/pCMV-myc constructs were made in a similar fashion, and the oligonucleotide primers were listed in Table 1.

Quantitation of viable cells with trypan blue dye exclusion assay and MTT assay

HEK293 cells seeding in a 24-well plate (Costar) were transfected with 7a/pEGFP-N1, pEGFP-N1, 7a/pCMV-myc and pCMV-myc in triplicate. At 12 h intervals after transfection, cells were rinsed with PBS and collected as single cell suspension by trypsinization. Viable cells, which were resistant to staining of trypan blue, were counted with hemacytometer chamber. To avoid bias, counting was done blindly for each sample by two researchers. At least three independent clones were analyzed.

For MTT assay, HEK 293 cells seeding in a 96-well plate (Costar) were transfected with different concentrations of 7a/pCMV-myc and pCMV-myc plasmids respectively in triplicate. After 48 h, each well was supplemented with 20 μl of MTT

Table 1
Primes used for wild-type and truncated 7a constructs[a]

Construct name	Polarity	Sequence[a]
7a/pEGFP-N1	Sense[b]	5′-CCGCTCGAGCGCCACCATGGGCAAAATTATTCTCTTCCTGACATTG-3′
	Antisense[c]	5′-CGGAATTCCTTCTGTCTTTCTCTTAATGGTGAAGC-3′
7a/pEGFP-C1	Sense	5′-CGCGAATTCCGCCACCATGAAAATTATTCTCTTCC-3′
	Antisense	5′-GCGGTCGACTCATTCTGTCTTTCTCTTAAT G-3′
7a/pCMV-myc	Sense	5′-CGCGAATTCGGATGAAAATTATTCTCTTCC-3′
	Antisense	5′-CCGCTCGAGTCATTCTGTCTTTCTCTTAATGGTGAAGC-3′
7a myc-D118–122	Sense	5′-CGCGAATTCGGATGAAAATTATTCTCTTCC-3′
	Antisense	5′-CGCGTCGACTCAAATGGTGAAGCAAAGTATTA-3′
7a myc-D102–122	Sense	5′-CGCGAATTCGGATGAAAATTATTCTCTTCC-3′
	Antisense	5′-CGCGTCGACTCAAAGTGGCGACTAGAGCTCTTG-3′
7a myc-D83–122	Sense	5′-CGCGAATTCGGATGAAAATTATTCTCTTCC-3′
	Antisense	5′-CGCGTCGACTCAAACTGATCTTGCACGCAGC-3′
7a myc-D44–122	Sense	5′-CGCGAATTCGGATGAAAATTATTCTCTTCC-3′
	Antisense	5′-CGCGTCGACTCAATTGCCCTCGTATGTTCC-3′

[a] Gene sequences correspond to SARS-CoV (ZJ01).
[b] Underlined nucleotides represent restriction site and Kozak sequence before start codon (ATG).
[c] Underlined nucleotides represent restriction site, and delete the stop codon.

solution (5 mg/ml), and continuously cultured for 4 h. The media were removed and 200 μl DMSO was added to each well. Then the plate was vibrated to dissolve crystals and was measured the optical density (O.D.) at 540 nm. The experiments were independently repeated three times.

Cell cycle analysis and apoptosis assay

For cell cycle analysis by flow cytometry, 2×10^6 cells transfected with 7a/pCMV-myc or 7a mutants/pCMV-myc were fixed with 70% cold ethanol at 4 °C overnight. Cells were then permeabilized in 0.1% Triton X-100/PBS, incubated with anti-myc antibody (1:100) and FITC-conjugated mouse anti-IgG (1:100) (Santa Cruz), then resuspended in propidium iodide (PI, 50 μg/ml) staining solution (containing DNase-free RNase A 20 μg/ml) for 30 min in the dark. Myc-tag was used to indicate positive and negative transfected cells, and cell cycle profile of two intercultural populations was analyzed by flow cytometry with CellQuest software (Becton Dickinson) (Deng et al., 2004). For the 7a/pEGFP-C1, 7a/pEGFP-N1 and pEGFP-N1 transfected cells, the fluorescence of GFP was used to indicate positive and negative transfected cells, and the cell cycle profiles were analyzed as before. The experiments were independently repeated three times.

For apoptosis assay, HEK293 cells seeding in a 24-well plate (Costar) were transfected with 7a/pCMV-myc, 7a mutants/pCMV-myc and pCMV-myc in triplicate. At the indicated times after transfection, cells were collected as single cell suspensions by trypsinization and incubated with Annexin V-FITC and PI according to the manufacturer's introductions (Clontech). The rates of apoptosis were analyzed by flow cytometry.

Confocal microscopy analysis

Cellular localization of SARS-CoV 7a protein and its mutants were prepared in transfected cells according to the procedure described before (Yuan et al., 2005).

For BrdUrd incorporation, Vero and COS-7 were transfected with 7a/pEGFP-N1 and pEGFP-N1 at 24 h after transfection. Cells on glass slip were incubated with 10 μmol/l BrdUrd for 4 h for 37 °C, and fixed with 100% methanol at 4 °C for 10 min. BrdUrd binding sites were exposed by treatment with 2 M hydrochloric acid at 37 °C for 2 h, and followed to neutralize in 0.1 M borate buffer (pH 8.5). After washing in PBS, cells were permeabilized in 0.1% Triton X-100/PBS for 5 min and incubated with anti-BrdUrd (1:100, Sigmal) and anti-GFP (1:100, Santa Cruz) antibodies for 1 h. Images were viewed and collected with confocal fluorescent microscope connected to a Bio-Rad Radiance 2100 laser scanner.

Western blot analysis

The transfected cells were harvested at given times after transfection. Total cell lysates preparation and Western blot analysis were performed according to the procedure described before (Yuan et al., 2004). In brief, the cell lysates were clarified by centrifugation at 12,000 × *g* for 10 min at 4 °C. Equal amounts of protein (20 μg) were separated by SDS-PAGE and transferred to NC membranes. The membranes were probed with primary antibodies (antibodies against myc, β-actin, cyclin D1, cyclin D2, anti-phospho-Rb on ser795 and ser809/811, CDK4, CDK6, cyclin D3, cdc2 and cyclin A were purchased from Cell Signaling) and followed by horseradish peroxidase-conjugated secondary antibody. Antibody detection was performed using an enhanced chemiluminescence (ECL) detection kit (Cell Signaling).

When it was necessary to reprobe the membrane with another antibody, the membrane was stripped with stripping buffer (2% SDS, 100 mM β-mercaptoethanol, 6.25 mM Tris–HCl pH 6.8) at 65 °C for 30 min and washed with TBS buffer before use.

RT-PCR assay

Total RNA was purified from 7a/pCMV-myc and pCMV-myc transfected HEK 293 cells. Reverse transcription-PCR (RT-PCR) was performed using the primes for cyclin D3 (sense primer, 5′-CCT CCT ACT TCC AGT GCG TG-3′; anti-sense primer, 5′-GCA ACT GGC GGG GAG AGA CA-3′) (299 bp) and β-actin (sense primer, 5′-CAC TCT TCC AGC CTT CCT TCC-3′; anti-sense primer, 5′-CGG ACT CGT CAT ACT CCT GCT T-3′) (338 bp) genes. The cycling conditions were as follows: 94 °C for 5 min, 30 s each at 94 °C, 62 °C and 72 °C for 35 cycles in a Perkin-Elmer-Cetus 2400 Gene-Amp PCR system. The PCR products were separated on 1.2% agarose gel.

Statistical analysis

Statistic analysis was performed using Student's *t* test. Data are reported as the mean and standard deviation.

Acknowledgments

We thank Prof. Shibo Jiang (New York Blood Center) for critical reading of the manuscript, Associated-Prof. Zhou Tao for the assay of confocal microscopy and Dr. Feng Yan-Bin, Liu Hong-Yan, Li Su-Yan and Yu Zu-yin for the construction of some plasmids and some help. This work was supported by a grant from the Nature Science Foundation of China (30470093).

References

Bonneau, A.M., Sonenberg, N., 1987. Involvement of the 24-kDa cap-binding protein in regulation of protein synthesis in mitosis. J. Biol. Chem. 262 (23), 11134–11139.

Chen, C.J., Makino, S., 2002. Murine coronavirus-induced apoptosis in 17Cl-1 cells involves a mitochondria-mediated pathway and its downstream caspase-8 activation and bid cleavage. Virology 302 (2), 321–332.

Chen, C.J., Makino, S., 2004. Murine coronavirus replication induces cell cycle arrest in G0/G1 phase. J. Virol. 78 (11), 5658–5669.

Chen, C.J., Sugiyama, K., Kubo, H., Huang, C., Makino, S., 2004. Murine coronavirus nonstructural protein p28 arrests cell cycle in G0/G1 phase. J. Virol. 78 (19), 10410–10419.

Deng, L.W., Chiu, I., Strominger, J.L., 2004. MLL 5 protein forms intranuclear foci, and overexpression inhibits cell cycle progression. Proc. Natl. Acad. Sci. U.S.A. 101 (3), 757–762.

Dimberg, A., Karlberg, I., Nilsson, K., Oberg, F., 2003. Ser727/Tyr701-phosphorylated Stat1 is required for the regulation of c-Myc, cyclins, and p27Kip1 associated with ATRA-induced G0/G1 arrest of U-937 cells. Blood 102 (1), 254–261.

Drosten, C., Gunther, S., Preiser, W., van der Werf, S., Brodt, H.R., Becker, S., Rabenau, H., Panning, M., Kolesnikova, L., Fouchier, R.A., et al., 2003. Identification of a novel coronavirus in patients with severe acute respiratory syndrome. N. Engl. J. Med. 348 (20), 1967–1976.

Fielding, B.C., Tan, Y.J., Shuo, S., Tan, T.H., Ooi, E.E., Lim, S.G., Hong, W., Goh, P.Y., 2004. Characterization of a unique group-specific protein (U122) of the severe acute respiratory syndrome coronavirus. J. Virol. 78 (14), 7311–7318.

Gemeniano, M.C., Sawai, E.T., Sparger, E.E., 2004. Feline immunodeficiency virus Orf-A localizes to the nucleus and induces cell cycle arrest. Virology 325 (2), 167–174.

He, J., Choe, S., Walker, R., Di Marzio, P., Morgan, D.O., Landau, N.R., 1995. Human immunodeficiency virus type 1 viral protein R (Vpr) arrests cells in the G2 phase of the cell cycle by inhibiting p34cdc2 activity. J. Virol. 69 (11), 6705–6711.

Herrewegh, A.A., Vennema, H., Horzinek, M.C., Rottier, P.J., de Groot, R.J., 1995. The molecular genetics of feline coronaviruses: comparative sequence analysis of the ORF7a/7b transcription unit of different biotypes. Virology 212 (2), 622–631.

Hofmann, H.J., Hadge, D., 1987. On the theoretical prediction of protein antigenic determinants from amino acid sequences. Biomed. Biochim. Acta 46 (11), 855–866.

Huang, J.L., Huang, J., Duan, Z.H., Wei, J., Min, J., Luo, X.H., Li, J.G., Tan, W.P., Wu, L.Z., Liu, R.Y., et al., 2005. Th2 predominance and CD8+ memory T cell depletion in patients with severe acute respiratory syndrome. Microbes. Infect. 7 (3), 427–436.

Jeffers, S.A., Tusell, S.M., Gillim-Ross, L., Hemmila, E.M., Achenbach, J.E., Babcock, G.J., Thomas Jr., W.D., Thackray, L.B., Young, M.D., Mason, R.J., et al., 2004. CD209L (L-SIGN) is a receptor for severe acute respiratory syndrome coronavirus. Proc. Natl. Acad. Sci. U.S.A. 101 (44), 15748–15753.

Ksiazek, T.G., Erdman, D., Goldsmith, C.S., Zaki, S.R., Peret, T., Emery, S., Tong, S., Urbani, C., Comer, J.A., Lim, W., et al., 2003. A novel coronavirus associated with severe acute respiratory syndrome. N. Engl. J. Med. 348 (20), 1953–1966.

Li, W., Moore, M.J., Vasilieva, N., Sui, J., Wong, S.K., Beme, M.A., et al., 2003. Angiotensin-converting enzyme 2 is a functional receptor for the SARS coronavirus. Nature 426 (6965), 450–454.

Marra, M.A., Jones, S.J., Astell, C.R., Holt, R.A., Brooks-Wilson, A., Butterfield, Y.S., Khattra, J., Asano, J.K., Barber, S.A., Chan, S.Y., 2003. The genome sequence of the SARS-associated coronavirus. Science 300 (5624), 1399–1404.

Nelson, C.A., Pekosz, A., Lee, C.A., Diamond, M.S., Fremont, D.H., 2005. Structure and intracellular targeting of the SARS-Coronavirus Orf7a accessory protein. Structure (Camb.) 13 (1), 75–85.

Nishioka, W.K., Welsh, R.M., 1994. Susceptibility to cytotoxic T lymphocyte-induced apoptosis is a function of the proliferative status of the target. J. Exp. Med. 179 (2), 769–774.

Paul, P.S., Vaughn, E.M., Halbur, P.G., 1997. Pathogenicity and sequence analysis studies suggest potential roles of gene 3 in virulence of swine enteric and respiratory coronavirus. Adv. Exp. Med. Biol. 412, 317–321.

Poutanen, S.M., Low, D.E., Henry, B., Finkelstein, S., Rose, D., Green, K., Tellier, R., Draker, R., Adachi, D., Ayers, M., et al., 2003. Identification of severe acute respiratory syndrome in Canada. N. Engl. J. Med. 348 (20), 1995–2005.

Rota, P.A., Oberste, M.S., Monroe, S.S., Nix, W.A., Campagnoli, R., Icenogle, J.P., Penaranda, S., Bankamp, B., Maher, K., Chen, M.H., et al., 2003. Characterization of a novel coronavirus associated with severe acute respiratory syndrome. Science 300 (5624), 1394–1399.

Sherr, C.J., Roberts, J.M., 1999. CDK inhibitors: positive and negative regulators of G1-phase progression. Genes Dev. 13 (12), 1501–1512.

Sicinska, E., Aifantis, I., Le Cam, L., Swat, W., Borowski, C., Yu, Q., Ferrando, A.A., Levin, S.D., Geng, Y., von Boehmer, H., Sicinski, P., 2003. Requirement for cyclin D3 in lymphocyte development and T cell leukemias. Cancer Cell 4 (6), 451–461.

Tan, Y.J., Fielding, B.C., Goh, P.Y., Shen, S., Tan, T.H., Lim, S.G., Hong, W., 2004a. Overexpression of 7a, a protein specifically encoded by the severe acute respiratory syndrome coronavirus, induces apoptosis via a caspase-dependent pathway. J. Virol. 78 (24), 14043–14047.

Tan, Y.J., Teng, E., Shen, S., Tan, T.H., Goh, P.Y., Fielding, B.C., Ooi, E.E., Tan, H.C., Lim, S.G., Hong, W., 2004b. A novel severe acute respiratory syndrome coronavirus protein, U274, is transported to the cell surface and undergoes endocytosis. J. Virol. 78 (13), 6723–6734.

Tsang, K.W., Ho, P.L, Ooi, G.C., Yee, W.K., Wang, T., Chan-Yeung, M., Lam, W.K., Seto, W.H., Yam, L.Y., Cheung, T.M., 2003. A cluster of cases of severe acute respiratory syndrome in Hong Kong. N. Engl. J. Med. 348 (20), 1977–1985.

Yount, B., Curtis, K.M., Fritz, E.A., Hensley, L.E., Jahrling, P.B., Prentice, E., Denison, M.R., Geisbert, T.W., Baric, R.S., 2003. Reverse genetics with a full-length infectious cDNA of severe acute respiratory syndrome coronavirus. Proc. Natl. Acad. Sci. U.S.A. 100 (22), 12995–13000.

Yuan, X., Cong, Y., Hao, J., Shan, Y., Zhao, Z., Wang, S., Chen, J., 2004. Regulation of LIP level and ROS formation through interaction of H-ferritin with G-CSF receptor. J. Mol. Biol. 339 (1), 131–144.

Yuan, X., Li, J., Shan, Y., Yang, Z., Zhao, Z., Chen, B., Yao, Z., Dong, B., Wang, S., Chen, J., Cong, Y., 2005. Subcellular localization and membrane association of SARS-CoV 3a protein. Virus Res. 109 (2), 191–202.